Please cite this article in press as: Huang and Chen, PIP2 regulation of TRPV4 channels: Binding sites and dynamic coupling, Biophysical Journal (2025), https://doi.org/10.1016/j.bpj.2025.08.006

Biophysical Journal
Article

Biophysical Society

PIP2 regulation of TRPV4 channels: Binding sites and dynamic coupling

Jian Huang[1] and Jianhan Chen[1,*]
[1]Department of Chemistry, University of Massachusetts, Amherst, Massachusetts

ABSTRACT Transient Receptor Potential subfamily V4 (TRPV4) is a nonselective cation channel that plays important roles in thermo-sensing, osmoregulation, nociception, and bone homeostasis. The activities of TRV4 channels are known to be regulated by phosphatidylinositol 4,5-bisphosphate (PIP2), even though its molecular basis remains poorly understood at present. Existing studies reveal great uncertainty or even controversy on the binding sites as well as functional effects of PIP2 on TRPV4. Analysis of available cryo-EM structures suggests that the previously proposed sites on the N-terminal domain and the ankyrin repeat domain are too distal from the membrane interface and thus unlikely to be the primary sites for PIP2 regulation. Instead, we have identified two possible PIP2 binding sites near the cytosolic membrane interface using structural analysis and molecular docking. Atomistic simulations and free energy analysis reveal that these two sites belong to a single broad binding groove, where PIP2 binding is dynamic and can sample multiple configurations of interactions with positively charged side chains within the groove. These local free energy minima are separated by small free energy barriers and offer ~4 kcal/mol stability with respect to the membrane bulk. Furthermore, dynamic network analysis suggests that PIP2 binding in the predicted groove can modulate the dynamic coupling between various domains of TRPV4, potentially priming the channel for responding to various stimuli. Together, these results provide important new insights on the possible molecular basis of PIP2 binding and regulation of TRPV4 activities.

SIGNIFICANCE PIP2 is a major regulatory lipid for many ion channels including the TRPV4 protein. There exists significant controversy in the binding site and effects of PIP2. In this work, structural analysis, docking, and atomistic simulations were combined to identify a single positively charged groove at the intracellular interface of TRPV4 that may be directly responsible for PIP2 binding. Atomistic simulations and free analysis suggest that binding of PIP2 is highly dynamic. Even though PIP2 binding does not induce a significant structural response, it can significantly enhance the dynamic coupling of various domains of TRPV4, potentially priming the protein to respond to various stimuli. These results provide important new insights on the possible molecular basis of PIP2 regulation of TRPV4.

INTRODUCTION

Ion channels are pore-forming integrated membrane proteins that are of great physiological importance (1). They respond to a myriad of cellular factors including membrane electric potential and binding of ligands and ions to control ion permeation across membranes and downstream signaling pathways (2–4). A thorough understanding of the molecular mechanisms underlying ion channel regulation is paramount for deciphering their roles in both normal and disease states and ultimately translating this knowledge into effective therapeutic interventions for channelopathies (5). Importantly, lipids within the surrounding membrane environment significantly influence ion channel function, playing crucial roles in protein oligomerization, assembly, and the modulation of the conformational energy landscape (6–8). Regulatory lipids such as phosphoinositides (PIPs), eicosanoids, and cholesterols have been shown to be involved in regulation of all major families of ion channels (9–11). Among them, phosphatidylinositol 4,5-bisphosphate (PIP2) is widely regarded as the most important one (9,12). It is a negatively charged lipid and is distributed preferentially in the cytoplasmic leaflet of the plasma membrane. Essentially all ion channels are affected by PIP2, including many potassium channels, voltage-gated sodium channels, calcium channels, and the transient receptor potential (TRP) channels (9,13–15).

TRP channels form the second largest ion channel family and play key roles in sensory perception (16,17). Virtually

Submitted March 9, 2025, and accepted for publication August 4, 2025.

*Correspondence: jianhanc@umass.edu

Editor: Ana Nicoleta Bondar.
https://doi.org/10.1016/j.bpj.2025.08.006

Please cite this article in press as: Huang and Chen, PIP2 regulation of TRPV4 channels: Binding sites and dynamic coupling, Biophysical Journal (2025), https://doi.org/10.1016/j.bpj.2025.08.006

all TRP channels are regulated by PIP2 (14,18). However, the functional effects of PIP2 regulation can vary drastically across TRP subfamilies and among different subfamily members (14), suggesting divergence in the underlying regulatory mechanisms. For example, within the TRPV subfamily, one of the most characterized TRP subfamilies, PIP2 has been shown to induce the activation of TRPV2 (19), TRPV5 (20,21), and TRPV6 (22–24), whereas it shows inhibitory effects for TRPV3 (25). Intriguingly, for TRPV4, an important TRPV member for sensing temperature, osmolarity, and mechanical force, PIP2 has been found to act as a coactivator for thermo-activation in single channel recording (26), whereas it was found to suppress TRPV4 channel activity in the whole-cell patch-clamp experiments (27) and in capillary endothelial cells (28). It is not clear how one may reconcile these contradictory observations, even though important differences do exist among the experimental approaches (e.g., whole-cell patch-clamp vs. excised inside-out patch-clamp and different cell types). Furthermore, two different PIP2 binding sites have been proposed for TRPV4, on the disordered N-terminal tail (K_{121}RWRK_{125}) and the ankyrin repeat domains (ARDs), respectively (26,27) (also see Fig. S1). Mutagenesis experiments did support a role of these putative sites in PIP2 regulation of TRPV4 (26,27). Yet, there exists substantial ambiguity in whether the observed functional effects are directly or indirectly related to PIP2 binding and regulation.

Existing structures of ion channels in complex with PIP2 have consistently identified intracellular membrane-facing grooves lined with positively charged residues as the binding sites (29–32). As illustrated in Fig. S2, the very first two cryo-EM structures of PIP2-bound potassium channels, Kir2.2 and Kir3.2, share a similar binding mode where PIP2 makes contacts with a cluster of positively charged residues located near the channel-inner membrane leaflet interface (29,30). Cryo-EM structures of PIP2-bound TRP members TRPM8 and TRPV5 also reveal a very similar mode of PIP2 binding (31,32). Furthermore, structural inspections (33,34) and in silico studies of TRPV1 (35–37) all consistently identified PIP2 binding to a positively charged groove near the intracellular membrane interface. With recent determination of high-resolution structures of TRPV4 (38–40), we now have a solid structural foundation for careful assessment of the previous proposed PIP2 binding sites and identification of other possible sites that may be more consistent with the established mode of PIP2 binding. Our analysis demonstrates that neither of the two previously proposed binding sites is close enough to the intracellular membrane interface to be a viable site for direct PIP2 binding and regulation. Instead, structural analysis followed by molecular docking identified two possible binding sites at the protein-inner leaflet membrane interfacial groove. We then performed free energy analysis to evaluate the binding affinity as well as relative importance of these two potential PIP2 binding sites, followed by molecular dynamics (MD) simulations to examine how PIP2 binding may affect the structure and dynamics of the TRPV4 protein. Together, our computational analysis provides important new insights into the molecular basis of PIP2 regulation of TRPV4 channels.

MATERIALS AND METHODS

Electrostatic potential surface calculation

The cryo-EM structures of hTRPV4 (38), in the apo (PDB: 8FC9), agonist-bound (PDB: 8FC9), and antagonist-bound states (PDB: 8FC7), were first processed using the PDB reader from the CHARMM-GUI web server (41) where all missing sidechains were constructed. The APBS tool in the PyMol software was then used to calculate the surface electrostatic potentials (42). All calculation parameters were set to be the default values with the potential range to be -5 to $+5$ K_bT/e_c, with 0 being the neutral electric potential.

N-terminal tail modeling and pulling simulation

To evaluate the ability of the K_{121}RWRK_{125} segment in the N-terminus as the PIP2 binding site (26), we first built the N-terminus tail (residues 120–145) that is absent in the hTRPV4 cryo-EM structure (PDB: 8FC7) using CHARMM (43). After short minimization and equilibration steps, a distance restraint from the MMFP module of CHARMM was applied to pull the z-position of the center of mass (COM) of the K_{121}RWRK_{125} segment to that of W737, which is the membrane-anchoring residue on the TRP helix and which marks the location of the intracellular membrane interface, as illustrated in Fig. S1. After the pulling phase, we removed the pulling MMFP potential and replaced it with a new distance restraint to restrain the z-distance of the middle residue W123 Cα atoms and the COM of W737 at 0 Å. The system was then run for 400 ps with a dielectric constant of 80. The MMFP distance restraint energy during the "holding" stage was extracted as an estimation of the energy cost of extending the K_{121}RWRK_{125} segment to reach the inner leaflet surface (Fig. S2).

Molecular docking

AutoDock4.2.6 and AutoDockTools were used for the molecular docking of PIP2 to potential binding sites on hTRPV4 (44–46). The cryo-EM structure of the antagonist-bound closed state of hTRPV4-RhoA (PDB: 8FC7) was used, because this structure has a better resolution of 3.30 Å and contains more resolved loops between transmembrane helices than the apo state structure (38). The original PDB file was preprocessed to remove other components (ions, lipids, and others) and only keep the protein components for the docking. Due to the C4 symmetry of the channel, only one protomer-membrane groove interface was set up as the search grid box. The atomic partial charges for the protein and ligand were processed using the Kollman charges and Gastegier charges, respectively (44). The genetic algorithm was used for pose searching during the docking (47,48). We chose to use the PIP2 (1-palmitoyl2-oleoyl-sn-glycero-phosphoinositide 4,5-bisphosphate), which has been previously parameterized to model the PIP2 ligand (49). The flexibility of the PIP2 ligand was set to only allow the following bonds rotatable: bonds connecting the hydroxyl groups and phosphate groups to the inositol ring, the glycerol backbone, and the C-C bonds in the last six carbons of the two tails. In total, 1000 docking trials were performed, and all poses were clustered using the K-means nearest neighbor algorithm (50) based on the COM locations of the PIP2 headgroups. Poses with the lowest binding free energies reported by the Autodock scoring function (51) from the four largest clusters were extracted as representative binding configurations. Based on their locations on the lipid leaflet, chemical environment, and also intuitions from previous reported cryo-EM

Please cite this article in press as: Huang and Chen, PIP2 regulation of TRPV4 channels: Binding sites and dynamic coupling, Biophysical Journal (2025), https://doi.org/10.1016/j.bpj.2025.08.006

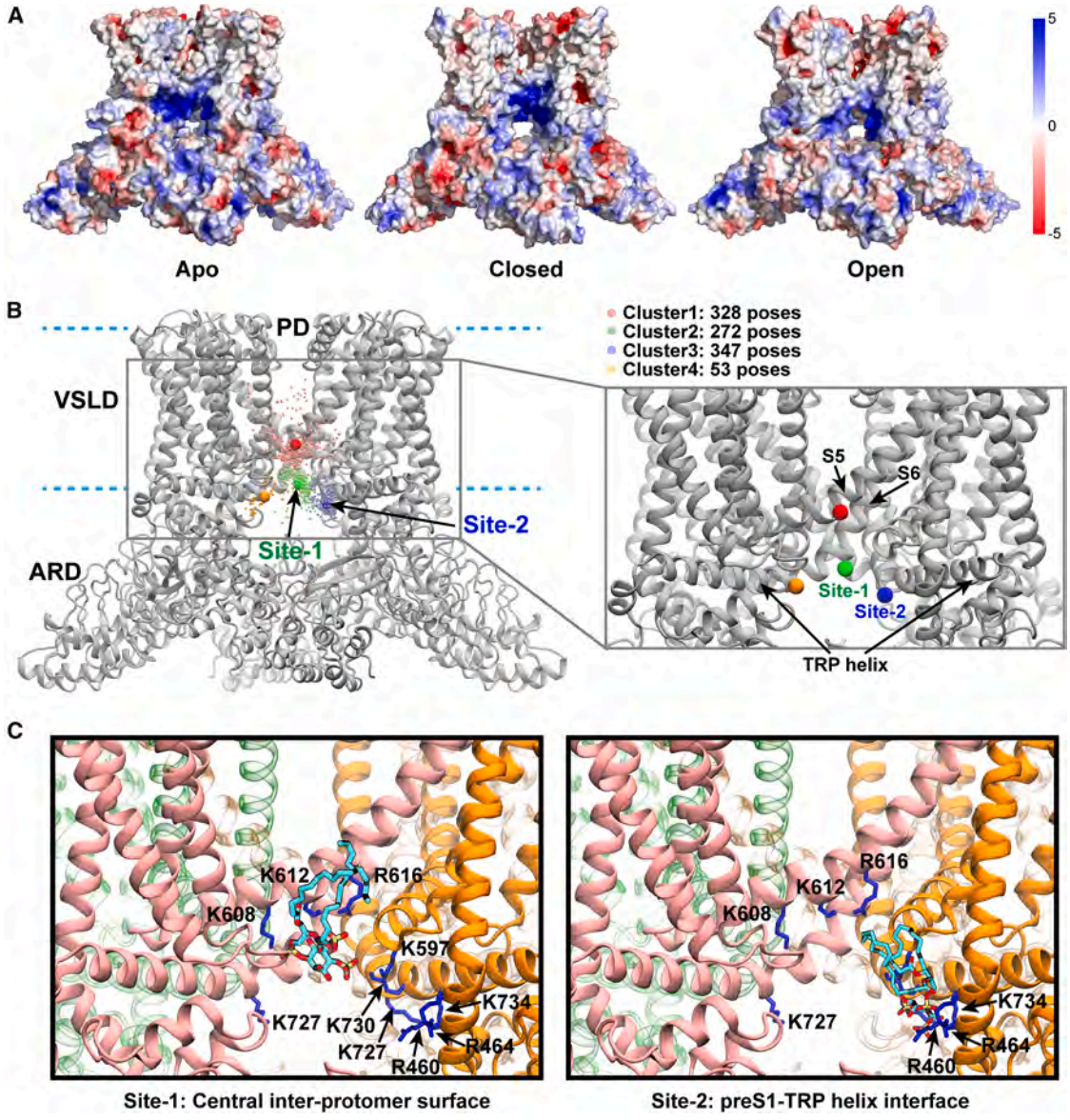

FIGURE 1 Potential PIP2-binding sites of hTRPV4. (*A*) Electrostatic potential surfaces of the apo, closed, and open structures of the hTRPV4 ion channel. The electrostatic potential is plot in the range of −5 to 5 K_bT/e_c with 0 being the neutral. (*B*) COM of the PIP2 headgroup from 1000 independent docking trials (*dot clouds*) and the four cluster centers from the K-means clustering (*blue, red, green, and orange spheres*). Inset shows a zoom-in view of the cluster centers. Blue dashed lines mark the location of membrane interfaces. Key domains, such as ankyrin repeats domain (ARD), voltage-sensing-domain-like domain (VSLD), and pore domain (PD), and key helices (S5, S6, and the TRP helix) are labeled. (*C*) Representative PIP2 binding poses from the green (site-1) and blue clusters (site-2). Two front protomers are shown using salmon and orange cartoons, whereas protomers in the back are shown as transparent cartoons. Positively charged residues within these sites are shown as blue sticks. The PIP2 molecules are shown in sticks with C, O, and P atoms colored with cyan, red, and yellow, respectively.

structures of ion channel-PIP2 complexes, only two sites were further investigated (see Fig. 1 and discussions in results).

Atomistic MD simulations

Given the selected docked poses with PIP2 bound to site-1 and site-2 (Fig. 1), initial structures with four PIP2s bound to all four pockets were created using the C4 symmetry operation. In addition, the unbound TRPV4 structure (the apo state) was derived from the closed-state hTRPV4 structure (PDB: 8FC7) after removing the bound ligands. These three initial structures were solvated with 1-palmitoyl-2-oleoylphosphatidylcholine (POPC) lipid bilayer and TIP3P water molecules using the CHARMM-GUI web server (41,52,53). Counter ions were added to neutralize the total charge, and 150 mM KCl was then added. The final simulation systems contain about 282,000 atoms with a dimension of 140 × 140 × 140 $Å^3$. The CHARMM36m protein and CHARMM36 lipid force fields were used to describe the systems (including PIP2) (54,55). All atomistic MD simulations were performed using the GPU-accelerated GROMACS 2019 (56,57). A cutoff of 12 Å was used for nonbonded force calculation with a smooth switching function starting at 10 Å. The Particle Mesh Ewald algorithm was used to calculate the electrostatic interactions (58). The

Please cite this article in press as: Huang and Chen, PIP2 regulation of TRPV4 channels: Binding sites and dynamic coupling, Biophysical Journal (2025), https://doi.org/10.1016/j.bpj.2025.08.006

SHAKE algorithm was used to constrain all hydrogen-involved chemical bonds (59) such that an integration step of 2 femtoseconds could be used.

To equilibrate the systems, 5000 steps of energy minimization were first performed, followed by a series of equilibration cycles where the heavy atoms of the protein and lipids (including both POPC and PIP2) were harmonically restrained with the force constant gradually reducing from 10 to 0.1 kcal/mol/Å^2. The systems were maintained at 298 K using the Berendsen thermostat (60), and all equilibration steps were performed under the NVT condition (constant particle number, constant volume, and constant temperature). For the production runs, all systems were performed under the NPT condition (constant particle number, constant pressure, and constant temperature) with the Nose-Hoover thermostat (61,62) and Parrinello-Rahman barostat (63). The temperature was set to 298 K; the pressure was 1 bar, imposed independently along z-axis and the x-y plane. The long missing loops between the S5 transmembrane (TM) helix and the pore-lining S6 helix (residues 639–661) were not modeled. Instead, we applied harmonical positional restraints on C_α atoms of residues 638 and 662 with a force constant of 1 kcal/mol/Å^2. For production, we performed three parallel 600-ns simulations of all three systems (numbered as sim#1, sim#2, and sim#3). Snapshots were saved every 50 ps.

For simulating the two additional local minima configurations of PIP2 binding captured during free energy calculations between site-1 and site-2, the initial configurations corresponding to these two minima (distances to site-2 are ∼3 and 5 Å) were extracted from the umbrella sampling trajectories (see below) and then used to initiate two replicas of unrestrained simulations of 300 ns in length using the same simulation setup as detailed above.

Umbrella sampling for relative free energy of PIP2 binding

Umbrella sampling (64) was used to calculate the potential of mean force (PMF) profiles of moving the bound PIP2 molecule from one binding site to the other (i.e., from site-1 to site-2 and from site-2 to site-1). The initial configurations of the two binding sites were obtained directly from the equilibrated configurations after the equilibration steps described above. In either moving direction, the COM of the PIP2 headgroup, which includes the inositol ring and phosphate groups, was restrained using harmonic distance restraint potentials with a force constant of 2 or 4 kcal/mol/Å^2, using the COM of the PIP2 headgroup in the target (final) binding site as the reference. A series of umbrella windows were simulated sequentially with distances being decreased by 2 Å per window. Each window was sampled for 50 ns, and the other simulation parameters or conditions were the same for all windows as the production simulations described above. The initial 5 ns of sampling of each window was removed, and only the remaining 45 ns of sampling was included in the weighted histogram analysis method (WHAM) (65) to derived the PMFs. Uncertainty of the calculated PMF profiles was evaluated using the differences between the first and second halves of the 45-ns sampling of all windows. Note that the distance restraints used in umbrella sampling simulations do not constrain the PIP2 molecule to move along any preset path, allowing better exploration of physically relevant states. By calculating the PMF from both directions, impacts of variability in the pulling paths on the convergence can be rigorously assessed.

Similar umbrella sampling protocol was used to calculate the PMF profile of PIP2 binding to site-1 with respect to the membrane bulk. For this, a steered MD simulation was first performed to generate the initial configurations with the COM of the PIP2 headgroup increasing from 0 (bound to site-1) to 30 Å (membrane bulk), along a directional vector defined by the COMs of TM helices and PIP2 headgroup bound in site-1. Umbrella sampling simulations were then performed for windows at separation distances increased by 2 Å per window. The sampling time was 50 ns each, and the distance restraint potential force constant was 2 kcal/mol. Additional windows at distances of 2.5 Å, 8 Å, 13.5 Å, and 22 Å were added with a higher force constant (4 kcal/mol) to ensure sufficient overlapping with their neighboring windows. The first 10 ns of the sampling data was removed to account for equilibration, whereas the rest was used to obtain the final PMF profile using WHAM. Uncertainty and convergence were evaluated using the block average method as mentioned above.

Structural and dynamic coupling analysis

All trajectories were aligned using the TM region (helix S1–S6) of hTRPV4 with respect to the equilibrated structure before further analysis. Root mean-squared deviations (RMSDs), root mean-squared fluctuations (RMSFs), and the COMs of the PIP2 headgroup were calculated using MDAnalysis (66). The contacting residues in trajectories were calculated by the GetContacts tool (https://getcontacts.github.io/). We used CHAP for pore radius calculation using only the 100- to 600-ns part of trajectories (67). Dynamic network analysis was performed using VMD (68) to determine dynamic coupling communities. The dynamic network analysis only included the 100- to 600-ns part of production trajectories. Trajectories from three parallel simulations were analyzed independently. To build the network, each amino acid was represented as a single node at the C_α position, and a contact (edge) was defined between two nodes if the minimal heavy-atom distance between residues was within a cutoff distance (4.5 Å) during at least 75% of the trajectory. The resulting contact matrix was weighted based on the covariance of dynamic fluctuation (C_{ij}) calculated from the same MD trajectory as $w_{ij} = -\log(|C_{ij}|)$. Contacts bridged by bound PIP2 were added to the network if two residues were both in contact with PIP2 for 50% of the simulation time. Communities calculated from the VMD dynamic network analysis of three parallel runs of each system were then grouped together based on their shared structural elements (Table S1).

RESULTS

Assessment and identification of possible PIP2 binding sites of hTRPV4

Two PIP2 binding sites have been previously proposed, the first one involving the N-terminal positively charged patch ($K_{121}RWRK_{125}$) (26) and the second one located at ankyrin repeat 4–5 fingers from ARD (27) (Fig. S1). Note that both sites were proposed before high-resolution structures became available first in 2018 (40). Given the latest Cryo-EM hTRPV4 structures (38,39), we first evaluate whether these two binding sites are physically close to potentially interact with PIP2 molecules residing in the inner membrane leaflet. The N-terminal loop is unresolved in the cryo-EM density map, presumably due to its disordered nature. As such, we first generated an extended conformation for the missing tail spanning residues 120 to 145 (Fig. S1 *A*) and then performed steered MD simulations to gently pull the positively charged patch toward the estimated position of the inner leaflet (see materials and methods). As shown by Fig. S1 *C*, the result suggests that, even though the $K_{121}RWRK_{125}$ patch could in principle reach the intracellular membrane interface, it requires the entirely disordered segment to be essentially fully extended and is thus highly unfavorable. For example, the restraint violation free energy is near 10 kcal/mol in order to hold the $K_{121}RWRK_{125}$ patch near the interface (Fig. S1 *C*). As such, the observed functional consequences of mutating or deleting patch

Please cite this article in press as: Huang and Chen, PIP2 regulation of TRPV4 channels: Binding sites and dynamic coupling, Biophysical Journal (2025), https://doi.org/10.1016/j.bpj.2025.08.006

$K_{121}RWRK_{125}$ is likely due to unknown indirect effects (26). Interestingly, Goretzki et al. have proposed a model where N-terminal patch binding to the membrane-bound PIP2 molecules could exert a pulling force that could promote the activation of TRPV4 channel based on coarse-grained simulations (69). Given the large force required for driving the extension of the N-terminal tail, such a direct mechanism involving patch $K_{121}RWRK_{125}$ remains to be further validated. The second binding site, the ARD4–5 finger loops, is simply too distant (∼40 Å) from the membrane interface to be capable of making any contacts with PIP2 in the inner leaflet surface (Fig. S1 *D*). Interestingly, the recently reported cryo-EM structures reveal that the RhoA GTPase binds to the same ARD surface (38,39), which should further prevent the ARD domain from engaging the inner leaflet and participate in PIP2 binding and regulation (Fig. S1 *D*).

Existing PIP2-bound ion channel structures consistently show that PIP2 binds to positively charged grooves near the interface of the inner leaflet (Fig. S2) (29–32). We wonder if similar grooves exist in the hTRPV4 structure. Intriguingly, there are four Arg and eight Lys residues clustered near the intracellular membrane interface (Fig. S3). Analysis of the electrostatic potential surfaces reveal a single positively charged groove on the surface of hTRPV4 near the intracellular membrane interface in the apo, agonist, and agonist-bound structures (Fig. 1 *A*). Such a groove resembles others observed previously (Fig. S2), strongly supporting the likelihood of binding negatively charged PIP2. Therefore, we performed molecular docking trials to predict possible PIP2 binding poses on this protein-inner leaflet interface (see materials and methods). Of the 1000 docking trials, there are roughly four major binding poses based on clustering of the locations of the COM of the PIP2 headgroup (Fig. 1 *B*). Upon further inspection of the cluster 1, it places the PIP2 headgroup into the unfavorable hydrophobic interior of membrane, probably because the Autodock scoring function does not consider constraints from the membrane during docking simulations. Cluster 4 is the least populated cluster, with only 53 out of all docking trails, and a closer check of all binding poses in this cluster suggests the number of coordinating lysine residues is generally fewer (usually from K536, K608, and K727) and more scattered for PIP2 binding. We chose to rule out those two clusters. The representative docked poses of PIP2 from clusters 2 and 3, denoted as site-1 and site-2, respectively, from here on, are shown in Fig. 1 *C*. Site-1 is in the "central interprotomer" surface, and site-2 is in the "preS1-TRP helix" surface. In both sites, the PIP2 headgroup is coordinated with four positively charged residues (K608, K612, R616, and K730 for site-1; R460, K597, K730, and K734 for site-2). Note that the binding mode and locations of site-1 and site-2 are similar to the PIP2 binding sites found in the TRPV5 and TRPM8 ion channel, respectively (31,32) (also see Fig. S2).

PIP2 interacts dynamically with TRPV4 in both site-1 and site-2

To further refine the interaction and evaluate the stability of PIP2 binding, we performed three independent 600-ns unrestrained atomistic MD simulations in explicit solvent for the docked structures with PIP2 bound in site-1 and site-2 (See materials and methods). Note that each simulation contains four independent copies of the PIP2 binding site, and the total effective sampling time is 7.2 μs per site with three independent simulations. We first characterized the stability of PIP2 binding by examining the lateral movements of bound PIP2 molecules, as reflected in the COM of the headgroup. As shown in Fig. 2 *A*, all bound PIP2s stayed near the initial locations derived from docking simulations and did not diffusion too far away. The average x-y distance of ∼1.0 Å in site-1 and ∼3.6 Å in site-2 indicates that binding to both sites provides significant stability. Examination of the distributions of the distance between the PIP2 headgroup and key contacting charged residues (Fig. S4 *A* and Video S1) as well as the RMSD of the PIP2 headgroup from the initial docked poses (Fig. S4 *B* and Video S2) reveals that the bound PIP2 molecules stayed stable for the whole simulation time after initial 30-ns relaxations from the docking poses. Compared with the lateral diffusion of the POPC molecules locating in similar positions as site-1 and site-2 from the apo system simulation (Fig. S5), PIP2 bound in both site-1 and site-2 shows three times narrower averaged diffusion area. The simulations also show that binding at the central interprotomer interface (site-1) is slightly more restrictive with narrower lateral diffusion areas compared with binding at the pre-S1/TRP interface (site-2), suggesting that binding to site-1 may be slightly more stable. This will be further examined using free energy analysis in the following section.

We further examined the PIP2-protein contacts in site-1 and site-2 from the unrestrained simulations to gain insights of key interactions for PIP2 binding. Fig. 2 *B* summarizes the frequencies of protein residues contacting the headgroup, glycerol backbone, and tails of PIP2. In general, more contacting residues with larger contacting frequencies to all parts of PIP2 were observed in site-1 than in site-2. The PIP2 headgroup forms stable interactions with four positively charged residues, of which three (K612, R616, and K730) are also present in the docking result (Fig. 1 *B*). Interestingly, K597, located between site-1 and site-2 and originally only contacting PIP2 in site-2 docking poses, readily repositioned its sidechain to form stable interactions with the headgroup in PIP2 bound in site-1 with ∼100% contacting frequency (Fig. 2 *B*). In comparison, PIP2 bound in site-2 has only two "anchoring" interactions, with residues R460 and K597. Intriguingly, PIP2 can make far more extensive contacts through its glycerol backbone with adjacent hydrophobic residues in site-1 than in site-2 (Fig. 2 *B*), which is likely a major contributing

Please cite this article in press as: Huang and Chen, PIP2 regulation of TRPV4 channels: Binding sites and dynamic coupling, Biophysical Journal (2025), https://doi.org/10.1016/j.bpj.2025.08.006

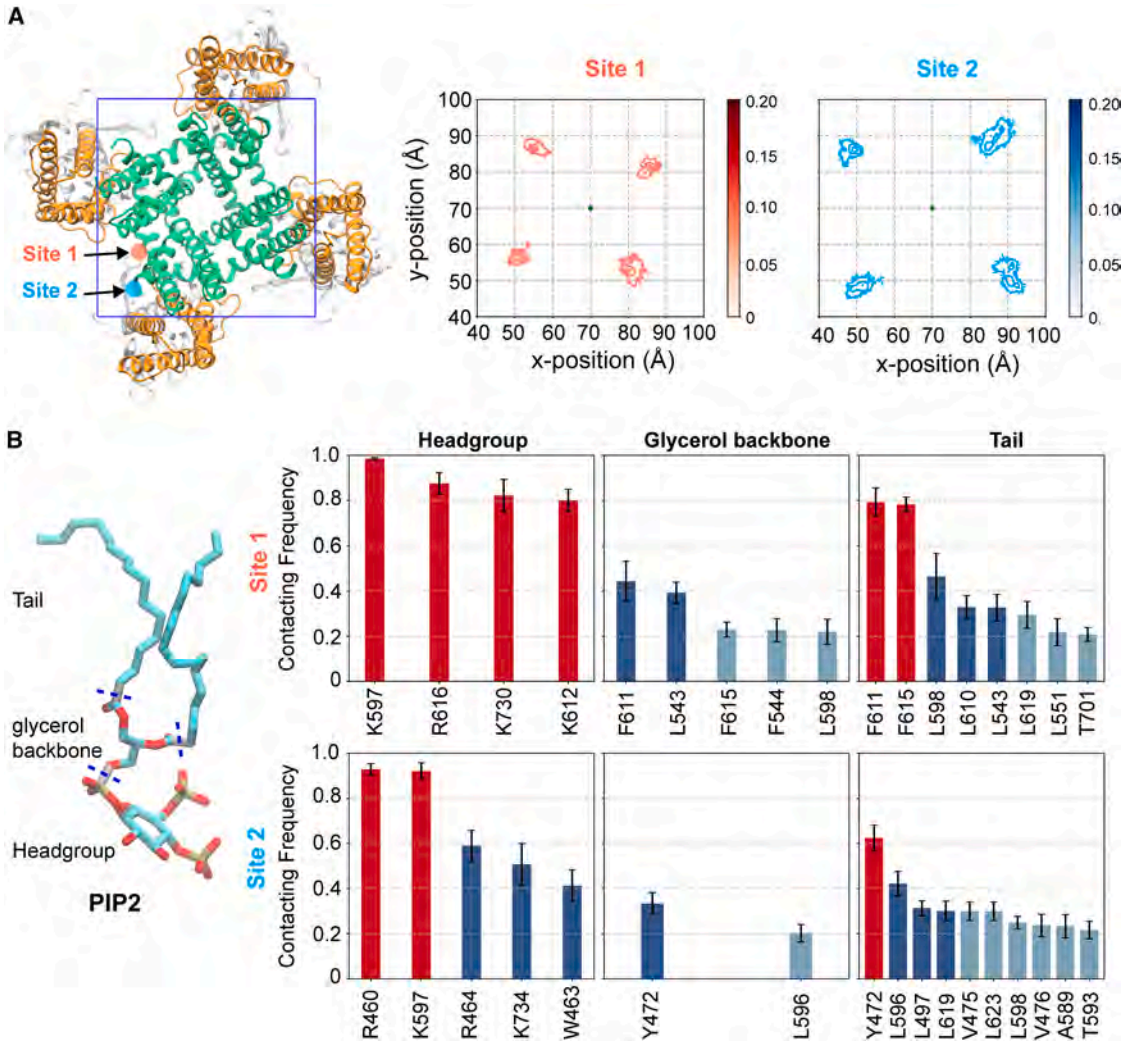

FIGURE 2 Dynamics and interactions of PIP2 in the two predicted binding sites of hTRPV4. (*A*) Lateral distributions of the COMs of the headgroups of PIP2 bound in site-1 (the central interprotomer surface) and site-2 (the pre-S1/TRP helix interface). Only the VSLDs (*orange*) and the pore domain (*green*) of hTRPV4 are shown in cartoon from the top. The blue square box marks the x-y range in the COM lateral distribution plots. Contours are drawn at 0.01, 0.04, 0.08, 0.12, and 0.2. (*B*) Residue contact frequencies calculated from combining all three equilibrium simulations of PIP2 bound in site-1 (*top row*) or site-2 (*bottom row*). PIP2 is divided into three parts: headgroup, glycerol backbone, and tail, shown by the left panel with C, O, and P colored with cyan, red, and yellow, respectively. In the bar plots, only residues with PIP2 contact frequencies larger than 0.2 are shown. The bars are colored red ($\geq$0.6), dark blue (<0.6 and $\geq$0.3), and light blue (<0.3 and $\geq$0.2). Error bars are standard errors derived from contact statistics of individual pockets (in total $4 \times 3 = 12$ pockets from three independent simulations).

factor of smaller lateral dynamics. In both sites, the nonpolar tails can make extensive but relatively unstable interactions with numerous hydrophobic residues above the charged sites. Overall, contacts revealed through atomistic simulations follow a similar pattern for PIP2 binding found in the previous PIP2-bound ion channel structures (Fig. S2) (29–32).

Both site-1 and site-2 have similar free energy stability for PIP2 binding

To quantify relative importance (or stability) PIP2 binding to site-1 and site-2, we calculated the PMF of PIP2 diffusion between these two sites. For this, a sequential umbrella sampling procedure with distance restraints imposed to gradually pull the COM of the PIP2 headgroup from site-1 to site-2 or from site-2 to site-1 in sampling windows was employed (Fig. 3 *A*; also see materials and methods). The sequential umbrella sampling procedure was necessary to allow adequate relaxation of the PIP2 tails as well as the surrounding lipid packing in response to PIP2 headgroup translocation. As shown in Fig. S4, the histograms show good overlaps throughout the sampling range. The resulting PMF profiles, summarized in Fig. 3 *B*, seem well converged and identify the two local minima that correspond to the two binding sites with a distance separation of 7∼9 Å. The free energy difference between the two sites is insignificant, regardless of whether site-1 or site-2 was used as the starting

Please cite this article in press as: Huang and Chen, PIP2 regulation of TRPV4 channels: Binding sites and dynamic coupling, Biophysical Journal (2025), https://doi.org/10.1016/j.bpj.2025.08.006

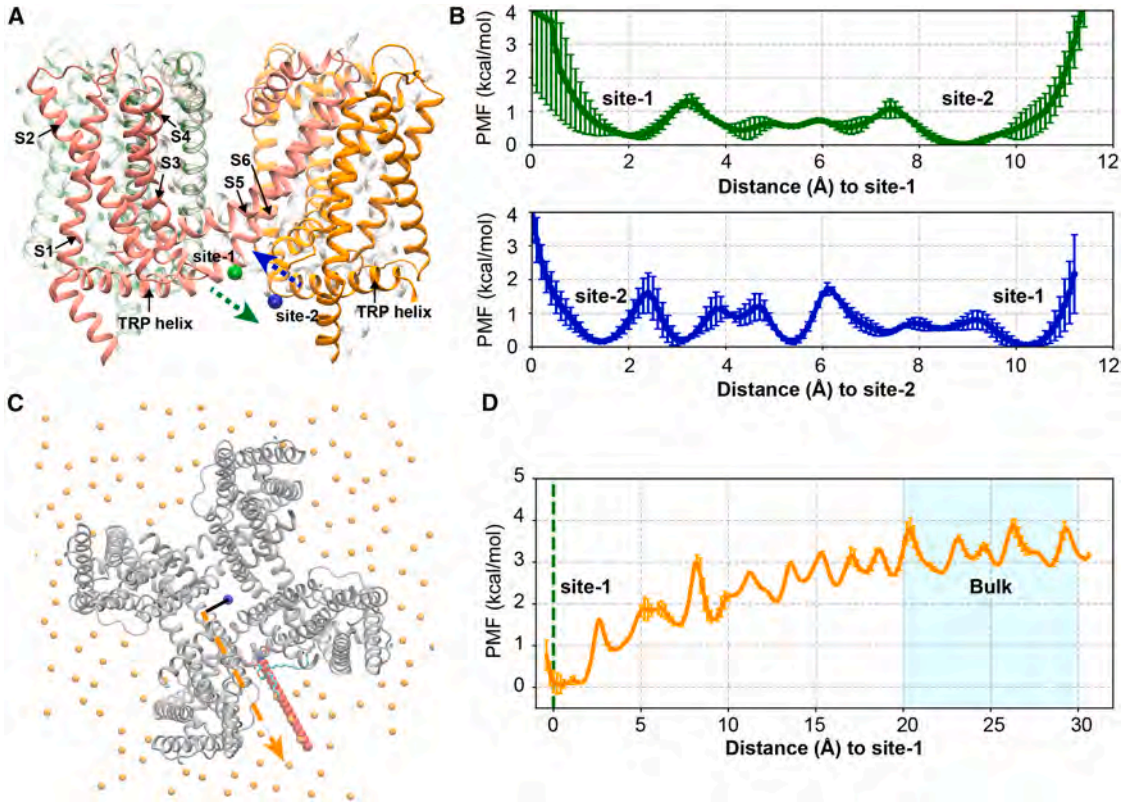

FIGURE 3 Free energy of PIP2 binding to site-1 and site-2. (*A*) Schematic illustration of two sets of umbrella sampling simulations with PIP2 sequentially pulled from one site to the other in both directions (*green arrow: site-1 to site-2; blue arrow: site-2 to site-1*). Only the pre-S1 helices and TM regions are shown in the cartoon for clarity. The initial COM positions of site-1 and site-2 are drawn as the green and blue spheres, respectively. (*B*) Free energy profiles of PIP2 translocation from site-1 to site-2 (*top panel*) and from site-2 to site-1 (*bottom panel*). (*C*) A top view of the cartoon representation of the transmembrane region of hTRPV4 (residue index: 450–750), illustrating the steered MD simulation for generating initial configurations of umbrella sampling (see materials and methods). Surrounding POPC lipids are marked with yellow spheres (for the phosphate groups) and the bound PIP2 in site-1 is shown with sticks. The initial headgroup COM locations for all umbrella sampling windows are shown as red spheres. (*D*) Free energy profile of PIP2 binding to site-1 with respect to the membrane bulk. Error bars are standard deviations calculated from the first and second halves of umbrella samplings.

or final state. The PMF profiles also reveal that there are only modest free energy barriers of 1–2 kcal/mol for PIP2 to diffuse between these two sites in both directions and further identify additional local minima with similar stabilities to site-1 and site-2 from docking simulations. We further calculated the PMF of PIP2 binding to site-1 with respect to the membrane bulk (Fig. 3 *D*). Note that the PMF does not reach a stable plateau even up to 30 Å from the binding site, which apparently reflects the granulous nature and slow diffusion dynamics of lipids and insufficient sampling of lipid diffusion within 50 ns of umbrella sampling. It has been shown that lipid diffusion is further slowed down near the membrane protein surface, often with ∼μs residence time (70–72). Therefore, we anticipate that it would require us ∼μs sampling time per umbrella window to eventually achieve a smooth PMF that flattens in the bulk. Despite the limited convergence of the PMF, the result suggests that binding to site-1 is approximately 3–4 kcal/mol stable with respect to the membrane bulk. Such a stability is generally consistent with the concentration of PIP2 (∼50 μM) used in experiments (26).

There are several minima and barriers between site-1 and site-2 corresponding to breaking and formation of salt bridges (Videos S3 and S4). Representative snapshots corresponding to the two middle local minima (d ∼ 3 Å and 5 Å) of pulling from site-2 to site-1 (blue curve in Fig. 3) show that phosphate groups of PIP2 in both locations form salt bridges with R460 and K597 (Fig. S7 and Videos S3 and S4). W463 providing polar contact in the first minimum (d ∼ 3 Å) was lost in the second minimum (d ∼ 5 Å), but a new salt bridge was formed with K612 (Fig. S7 and Videos S3 and S4). As such, breaking old salt bridges can quickly be compensated for by new salt bridges, resulting in the modest free energy barriers and several local minima. Indeed, when initiated from local minima observed in the PMFs, spontaneous transitions were observed in two of the four 300-ns trajectories (Fig. S8). The implication of these observations is that the site-1 and site-2 together may be classified as a broad PIP2 binding groove, where PIP2 binds dynamically and can sample several states with comparable stabilities. Multiple different PIP2 binding sites have also been reported in the Kir2.1 channel, where

Please cite this article in press as: Huang and Chen, PIP2 regulation of TRPV4 channels: Binding sites and dynamic coupling, Biophysical Journal (2025), https://doi.org/10.1016/j.bpj.2025.08.006

dynamic PIP2 binding is suggested to regulate the channel activity cooperatively (73). The breath of the site-1/site-2 groove also raises the possibility of more than one PIP2 binding simultaneously on hTRPV4 to cooperatively regulate hTRPV4 functions. Interestingly, in a recent cryo-EM structure of ATP-sensitive potassium (K_{ATP}) channel, two PIP2 molecules in the complex are found to bind to the channel protein adjacently, where one PIP2 is the canonical activation site, and another is proposed to play a regulatory role (74).

PIP2 binding modulates dynamic coupling of hTRPV4

To further understand the consequence of PIP2 binding on TRPV4 structure and dynamics, we analyze structural and dynamic properties among the apo, PIP2-bound state 1 (PIP2 binding in site-1), and PIP2-bound state 2 (PIP2 binding in site-2) states during the three independent 600-ns equilibrium simulations (see materials and methods). As shown in Fig. S9 *A*, all three systems exhibit stable RMSD (∼2 Å) for the TM region throughout the simulation timescale in all replicas. There appears to be minimal structural changes in response to PIP2 binding (Fig. S9 *C*). Consistent with a lack of significant structural changes, the pore radius profiles are very similar in all three states (Fig. S10). Comparison of the residue RMSF profiles shows that the cytosolic ARD domains have slightly bigger fluctuations than the TM domain (Fig. S9 *B*), but there is little difference between apo and the two PIP2-bound states. Even though the limited simulation timescale of 600 ns may not be enough to sample PIP2-induced conformational changes, the absence of direct response is probably not surprising given the apparent dynamic nature of PIP2/hTRPV4 interactions. Furthermore, a lack of direct PIP2-induced structural response is also apparently consistent with the experimental observations that PIP2 binding alone does not activate the TRPV4 channel (26).

The proposed PIP2 binding groove locates at the interface of two neighboring protomers and connects the TM domain to the TRP helix, a critical interfacial bridging element among voltage-sensing-domain-like domain (VSLD), pore domain (PD), and the coupling domain and has been proposed to play important roles in TRP channel gating and activation (75). It is thus possible that PIIP2 binding, albeit dynamic, could modulate dynamic coupling of the TRPV4 protein. For this, we constructed dynamic networks using the covariance matrices derived from MD trajectories and determined dynamic communities where the motions of residues are more strongly coupled to one another than the rest of the channel (see materials and methods). As illustrated in Fig. 4 *A*, dynamic communities are frequently localized to separate structural domains, such as individual VSLDs and ARDs, but they can also involve structural elements from different domains at the protomer or TM/ARD interfaces. Notably, the pore communities usually involve structural elements from all four protomers (e.g., light purple community in Fig. 4 *A*). Based on the general patterns among all simulation trajectories, dynamic communities of TRPV4 largely involve different combinations of a set of common structural elements (Fig. 4 *B*; Tables S1–S3). Each protomer could be roughly divided into ARD communities, TM communities (VSLD domain plus the S5–6 pore-forming helices), and coupling domain communities (consisting of the region between ARD and the S1 helix, plus the C-terminal domain after the TRP helix; colored in orange in Fig. 4 *B*).

We then focused on analyzing on TRP helix-involved communities from all trajectories of the apo, PIP2-bound to site-1 and site-2 states. In total, nine out of 12 (4×3) TRP helices from the three independent trajectories participate in dynamic communities as a whole helix, integrated with either the VSLD (plus the S4–5 linker) or the coupling domain in the apo state (the left panel in Fig. 4 *C*; Table S1). This indicates the TRP helix, even though lying on the interface between VSLD and the coupling domain, is insufficient to couple the dynamics of those two domains. The VSLD and the coupling domain are largely uncoupled in the apo system. In contrast, when PIP2 is bound to either site-1 or site-2, dynamic network analysis frequently "split" the TRP helix into two halves (11 out of 12 in the PIP2-bound to site-1 simulations and 10 out of 12 in the PIP2-bound to site-2 state), as illustrated in Fig. 4 *B*. In these cases, the first half TRP helix usually belongs in the same dynamic community with the VSLD domain and the S4–5 linker together, whereas the second half TRP helix belongs to a separate community with the coupling domain (and sometimes plus the lower half of the S1 helix; see Tables S2 and S3). Since the TRP segment remains a single helix structurally, the implication is that the TM and cytosolic domains of TRPV4 are more tightly coupled through the TRP helix when PIP2 is bound to either site-1 or site-2. The enhanced coupling could prime the channel to better transduce effects of various stimuli such as heat or agonist binding to the PD for activation of the channel.

We further examine the TM region to dissect the effects of PIP2 binding to the pore and VSLD dynamic coupling. In the apo state, there are four cases (out of 12) where the VSLD domains do not couple with the neighboring pore-forming helices S5–6 at all (Table S1), whereas only two such cases were found when PIP2 is bound to site-1 (Table S2). Strikingly, all VSLD domains in PIP2-bound to site-2 simulations are coupled with their neighboring pore-forming S5–6 helices, through the S4–5 linker (Table S3), as illustrated in the VSLD-PD communities in the right panel of Fig. 4 *D*. On the other hand, we found only localized "pore communities" in the apo state (Table S1 and the left panel of Fig. 4 *D*), which are formed by the S4–5 linker and the neighboring S5–6 helices (sometime plus the TRP helix) and segregated from other

Please cite this article in press as: Huang and Chen, PIP2 regulation of TRPV4 channels: Binding sites and dynamic coupling, Biophysical Journal (2025), https://doi.org/10.1016/j.bpj.2025.08.006

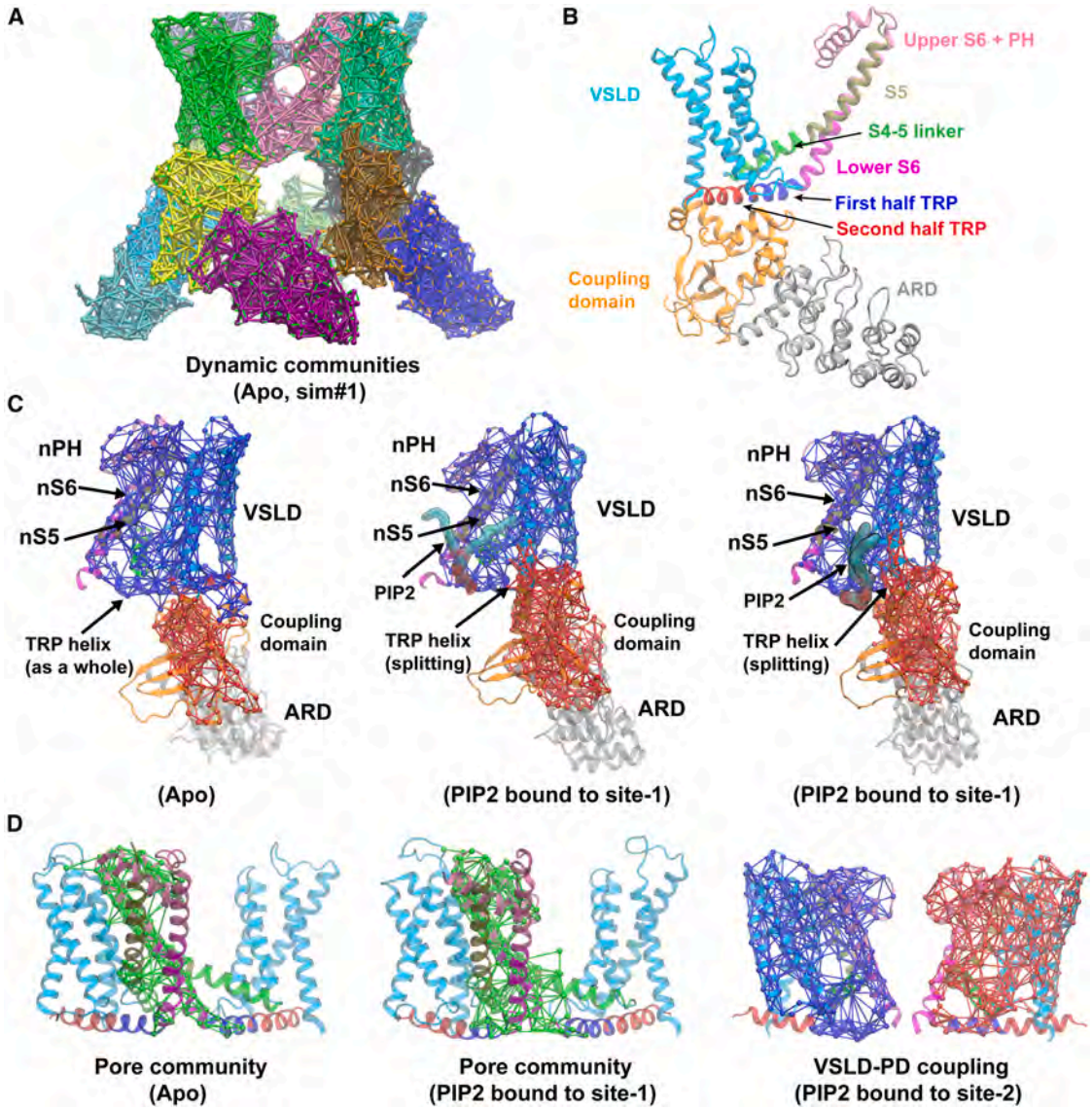

FIGURE 4 Dynamic coupling of hTRPV4 in apo and PIP2-bound states. (*A*) Representative dynamic communities derived from analysis of sim#1 of the apo state. (*B*) Structural elements frequently observed to form dynamic communities of the apo and PIP2-bound states (Tables S1–S3). (*C*) Representative TRP helix involving communities in three states. The ARD, coupling domain, VSLD from one monomer, and neighboring S5, pore helix (PH), and S6 (labeled as nS5, nPH, and nS6) are shown using the same coloring scheme as in Fig. 4 *A*. Two communities containing the VSLD-PD and the coupling domain are shown in blue and red meshes, respectively. PIP2 molecules are shown as sticks with transparent surfaces. (*D*) Representative localized pore communities from the apo and PIP2 bound to site-1 states (*green meshes*) and two VSLD-PD communities from the PIP2-bound to site-2 state (*blue and red meshes*).

domains, such as the VSLD and coupling domains. These observations indicate that PIP2 binding promotes stronger couplings between the PD and the surrounding VSLD domains, potentially priming the channel activation in response to external stimuli.

DISCUSSION

Membrane lipids shape the environment of ion channels and contribute to their assembly, stability, and regulation in profound ways. PIP2, in particular, has been shown to be a major signaling lipid frequently involved in ion channel regulation (9,13,14). For TRPV4 channels, existing studies have suggested contradictory regulatory effects of PIP2 (26–28) and further identified multiple possible PIP2 binding sites in the cytosolic ARD domain and N-terminal tail (26,27). Analysis based on recent cryo-EM structures demonstrate that these sites are spatially distal from the membrane and unlikely to be directly responsible for PIP2 binding and regulation. Instead, we show that a single positively charged groove exists on the TRPV4 surface near the intracellular membrane interface, similar to previously

Please cite this article in press as: Huang and Chen, PIP2 regulation of TRPV4 channels: Binding sites and dynamic coupling, Biophysical Journal (2025), https://doi.org/10.1016/j.bpj.2025.08.006

reported PIP2 binding sites in bound structures of several ion channels (13,30–32). Docking followed by atomistic simulations further resolved two possible PIP2 binding, at the "central interprotomer" (site-1) and "preS1-TRP helix" (site-2) surfaces (Fig. 1). PIP2 binding in these sites is dynamic, where the negatively charged headgroup can exchange interactions with multiple positively charged side chains. Free energy calculations revealed binding at site-1 and site-2 offers similar stability and identified additional intermediate states with similar PIP2 binding affinities. As such, the intracellular interface groove of TRPV4 should be considered a single, broad PIP2 binding site, which could potentially support binding of multiple PIP2 molecules. It was further determined that the broad binding site provides ∼4 kcal/mol stability relative to the membrane bulk. Notably, the site-1 binding mode is similar to the previously reported PIP2 binding in TRPV5 (31), where basal concentration PIP2 supports the constitutive opening of the channel. The site-2 binding is reminiscent of the PIP2 binding in TRPM8, which can also be activated by PIP2 (32). Further experiments such as mutagenesis and structural studies will be required to validate and resolve the molecular basis of PIP2 regulation of TRPV4 channels.

To examine if the PIP2 coordinating residues are conserved, we performed structure-based multisequence alignment using current available high-resolution structures of TRP channels that contain the TRP helix (see supporting material; Table S4). PIP2-coordinating positively charged residues identified in the groove of TRPV4 show different levels of conservation: K608 and K734 are the most conserved residues across all members except TRPA1; R464, K612, and R616 are mostly conserved within the TRPV subfamily members; other sites such as R460, K597, and K730 are not conserved. Therefore, site-1 is conserved within the TRPV subfamily members, but site-2 is not. Nevertheless, the PIP2-binding motifs formed by sequence-separated but structurally close residues usually do not need to be conserved, which has been shown before in a study of PIP2 regulation of the TRPM8 channel (32). Considering PIP2 regulation effects on different TRP channels can vary substantially, TRP channels likely have evolved to adopt different coordinating residues and different PIP2 regulation mechanisms across families as well as between members of the same subfamily.

Atomistic simulations in the current work did not reveal any significant conformational changes in response to PIP2 binding, which is consistent with the experimental observation that PIP2 binding alone does not activate the channel (26). However, dynamic network analysis revealed significant impacts of PIP2 binding in the dynamic coupling of the TRPV4 channel. PIP2 binding to either site-1 or site-2 enhances the dynamic coupling between the TM and cytosolic domains of TRPV4, potentially priming the channel to respond to various stimuli. Furthermore, binding to the "preS1-TRP helix" site (site-2) dramatically enhances the coupling between the VSLD and pore helices, which could also facilitate the pore activation. It is possible that under physiological conditions, PIP2 could bind to either site-1 or site-2 (or even both) depending on the cellular context such as the presence of another agonist or antagonist. The apparent complexity and plasticity of PIP2 binding may also explain why there have been controversial observations about whether PIP2 is inhibiting or activating in the hTRPV4 channel (27,28,37). Further experiments are required to further resolve these observations. Improved understanding of the molecular basis of PIP2 regulation in TRV4 channel function will pave the way for future studies of TRPV4 regulation. For example, single-channel recording has demonstrated that PIP2 binding and temperature together can activate hTRPV4 (26). Therefore, one could perform long-timescale atomistic simulations of TRPV4 at different temperatures in the PIP2-bound state to directly probe the mechanism and process of thermal activation. Another future direction would be to include more complex lipid environment in our simulation, such as PI(3,4)P2, PI(3,4,5)P2, and cholesterols, to more faithfully represent the real biologically relevant microenvironment of TRPV4 and resolve dynamics from competitive binding (27). Together with mutagenesis and functional studies, these efforts could reveal the precise regulatory and activation mechanisms of the hTRPV4 channel.

ACKNOWLEDGMENTS

The authors thank Drs. Jianmin Cui and Lu Zhao for constructive discussions during the early stage of this work. This work was supported by the National Institutes of Health Grant R35 GM144045 (to J.C.).

AUTHOR CONTRIBUTIONS

J.H. and J.C., conception and design of the study; J.H., performing the simulation; J.H. and J.C., analysis and interpretation of data, drafting and revising the manuscript.

DECLARATION OF INTERESTS

The authors declare no competing interests.

SUPPORTING MATERIAL

Supporting material can be found online at https://doi.org/10.1016/j.bpj.2025.08.006.

REFERENCES

1. Hille, B. 2001. Ion Channels of Excitable Membranes. Third edit Sinauer Associates.
2. Keynes, R. D. 1975. The Ionic Channels in Excitable Membranes. Ciba Found Symp, pp. 191–203.
3. Hebert, S. C. 1998. General principles of the structure of ion channels. *Am. J. Med.* 104:87–98.

Please cite this article in press as: Huang and Chen, PIP2 regulation of TRPV4 channels: Binding sites and dynamic coupling, Biophysical Journal (2025), https://doi.org/10.1016/j.bpj.2025.08.006

4. Minor, D. L. 2010. Chapter 30 - An Overview of Ion Channel Structure. *In* Handbook of Cell Signaling, Second Edition. R. A. Bradshaw and E. A. Dennis, eds Academic Press, San Diego, pp. 201–207.
5. Bagal, S. K., A. D. Brown, …, N. A. Swain. 2013. Ion Channels as Therapeutic Targets: A Drug Discovery Perspective. *J. Med. Chem.* 56:593–624.
6. Jodaitis, L., T. van Oene, and C. Martens. 2021. Assessing the Role of Lipids in the Molecular Mechanism of Membrane Proteins. *Int. J. Mol. Sci.* 22:7267.
7. Duncan, A. L., W. Song, and M. S. P. Sansom. 2020. Lipid-Dependent Regulation of Ion Channels and G Protein–Coupled Receptors: Insights from Structures and Simulations. *Annu. Rev. Pharmacol. Toxicol.* 60:31–50.
8. Corradi, V., B. I. Sejdiu, …, D. P. Tieleman. 2019. Emerging Diversity in Lipid-Protein Interactions. *Chem. Rev.* 119:5775–5848.
9. Hille, B., E. J. Dickson, …, B.-C. Suh. 2015. Phosphoinositides regulate ion channels. *Biochim. Biophys. Acta.* 1851:844–856.
10. Levitan, I., Y. Fang, …, V. Romanenko. 2010. Cholesterol and ion channels. *Subcell. Biochem.* 51:509–549.
11. Falkenburger, B. H., J. B. Jensen, …, B. Hille. 2010. Phosphoinositides: lipid regulators of membrane proteins. *J. Physiol.* 588:3179–3185.
12. van den Bogaart, G., K. Meyenberg, …, R. Jahn. 2011. Membrane protein sequestering by ionic protein–lipid interactions. *Nature.* 479: 552–555.
13. Rodríguez Menchaca, A. A., S. K. Adney, …, D. E. Logothetis. 2012. Dual Regulation of Voltage-Sensitive Ion Channels by PIP2. *Front. Pharmacol.* 3:170.
14. Rohacs, T. 2014. Phosphoinositide regulation of TRP channels. *Handb. Exp. Pharmacol.* 223:1143–1176.
15. Suh, B.-C., and B. Hille. 2008. PIP2 is a necessary cofactor for ion channel function: How and why? *Annu. Rev. Biophys.* 37:175–195.
16. Gees, M., G. Owsianik, …, T. Voets. 2012. TRP Channels. *Compr. Physiol.* 2:563–608.
17. Cao, E. 2020. Structural mechanisms of transient receptor potential ion channels. *J. Gen. Physiol.* 152:e201811998.
18. Taberner, F. J., G. Fernández-Ballester, …, A. Ferrer-Montiel. 2015. TRP channels interaction with lipids and its implications in disease. *Biochim. Biophys. Acta Biomembr.* 1848:1818–1827.
19. Mercado, J., A. Gordon-Shaag, …, S. E. Gordon. 2010. Ca2+-dependent desensitization of TRPV2 channels is mediated by hydrolysis of phosphatidylinositol 4,5-bisphosphate. *J. Neurosci.* 30:13338–13347.
20. Lee, J., S.-K. Cha, …, C.-L. Huang. 2005. PIP2 activates TRPV5 and releases its inhibition by intracellular Mg2+. *J. Gen. Physiol.* 126:439–451.
21. Rohács, T., C. M. B. Lopes, …, D. E. Logothetis. 2005. PI(4,5)P2 regulates the activation and desensitization of TRPM8 channels through the TRP domain. *Nat. Neurosci.* 8:626–634.
22. Thyagarajan, B., V. Lukacs, and T. Rohacs. 2008. Hydrolysis of phosphatidylinositol 4,5-bisphosphate mediates calcium-induced inactivation of TRPV6 channels. *J. Biol. Chem.* 283:14980–14987.
23. Zakharian, E., C. Cao, and T. Rohacs. 2011. Intracellular ATP supports TRPV6 activity via lipid kinases and the generation of PtdIns(4,5) P_2. *FASEB J.* 25:3915–3928.
24. Cao, C., E. Zakharian, …, T. Rohacs. 2013. Interplay between calmodulin and phosphatidylinositol 4,5-bisphosphate in Ca2+-induced inactivation of transient receptor potential vanilloid 6 channels. *J. Biol. Chem.* 288:5278–5290.
25. Doerner, J. F., H. Hatt, and I. S. Ramsey. 2011. Voltage- and temperature-dependent activation of TRPV3 channels is potentiated by receptor-mediated PI(4,5)P2 hydrolysis. *J. Gen. Physiol.* 137:271–288.
26. Garcia-Elias, A., S. Mrkonjić, …, M. A. Valverde. 2013. Phosphatidylinositol-4,5-biphosphate-dependent rearrangement of TRPV4 cytosolic tails enables channel activation by physiological stimuli. *Proc. Natl. Acad. Sci. USA.* 110:9553–9558.
27. Takahashi, N., S. Hamada-Nakahara, …, S. Suetsugu. 2014. TRPV4 channel activity is modulated by direct interaction of the ankyrin domain to PI(4,5)P_2. *Nat. Commun.* 5:4994.
28. Harraz, O. F., T. A. Longden, …, M. T. Nelson. 2018. PIP2 depletion promotes TRPV4 channel activity in mouse brain capillary endothelial cells. *eLife.* 7:e38689.
29. Hansen, S. B., X. Tao, and R. MacKinnon. 2011. Structural basis of PIP2 activation of the classical inward rectifier K+ channel Kir2.2. *Nature.* 477:495–498.
30. Niu, Y., X. Tao, …, R. MacKinnon. 2020. Cryo-EM analysis of PIP2 regulation in mammalian GIRK channels. *eLife.* 9:e60552.
31. Hughes, T. E. T., R. A. Pumroy, …, V. Y. Moiseenkova-Bell. 2018. Structural insights on TRPV5 gating by endogenous modulators. *Nat. Commun.* 9:4198.
32. Yin, Y., S. C. Le, …, S.-Y. Lee. 2019. Structural basis of cooling agent and lipid sensing by the cold-activated TRPM8 channel. *Science.* 363: eaav9334.
33. Cao, E., L. M, …, D. J. 2013. TRPV1 structures in distinct conformations reveal activation mechanisms. *Nature.* 504.
34. Liao, M., E. Cao, …, Y. Cheng. 2013. Structure of the TRPV1 ion channel determined by electron cryo-microscopy. *Nature.* 504:107–112.
35. Brauchi, S., G. Orta, …, R. Latorre. 2007. Dissection of the components for PIP2 activation and thermosensation in TRP channels. *Proc. Natl. Acad. Sci. USA.* 104:10246–10251.
36. Zheng, W., and H. Wen. 2021. Predicting lipid and ligand binding sites in TRPV1 channel by molecular dynamics simulation and machine learning. *Proteins.* 89:966–977.
37. Poblete, H., I. Oyarzún, …, R. Latorre. 2015. Molecular Determinants of Phosphatidylinositol 4,5-Bisphosphate (PI(4,5)P2) Binding to Transient Receptor Potential V1 (TRPV1) Channels. *J. Biol. Chem.* 290:2086–2098.
38. Kwon, D. H., F. Zhang, …, S.-Y. Lee. 2023. TRPV4-Rho GTPase complex structures reveal mechanisms of gating and disease. *Nat. Commun.* 14:3732.
39. Nadezhdin, K. D., I. A. Talyzina, …, A. I. Sobolevsky. 2023. Structure of human TRPV4 in complex with GTPase RhoA. *Nat. Commun.* 14:3733.
40. Deng, Z., N. Paknejad, …, P. Yuan. 2018. Cryo-EM and X-ray structures of TRPV4 reveal insight into ion permeation and gating mechanisms. *Nat. Struct. Mol. Biol.* 25:252–260.
41. Jo, S., T. Kim, …, W. Im. 2008. CHARMM-GUI: a web-based graphical user interface for CHARMM. *J. Comput. Chem.* 29:1859–1865.
42. Baker, N. A., D. Sept, …, J. A. McCammon. 2001. Electrostatics of nanosystems: application to microtubules and the ribosome. *Proc. Natl. Acad. Sci. USA.* 98:10037–10041.
43. Brooks, B. R., C. L. Brooks, …, M. Karplus. 2009. CHARMM: The Biomolecular Simulation Program. *J. Comput. Chem.* 30:1545–1614.
44. Morris, G. M., R. Huey, …, A. J. Olson. 2009. AutoDock4 and AutoDockTools4: Automated Docking with Selective Receptor Flexibility. *J. Comput. Chem.* 30:2785–2791.
45. Cosconati, S., S. Forli, …, A. J. Olson. 2010. Virtual Screening with AutoDock: Theory and Practice. *Expet Opin. Drug Discov.* 5:597–607.
46. Forli, S., and A. J. Olson. 2012. A force field with discrete displaceable waters and desolvation entropy for hydrated ligand docking. *J. Med. Chem.* 55:623–638.
47. Fraser, A. 1957. Simulation of Genetic Systems by Automatic Digital Computers II. Effects of Linkage on Rates of Advance Under Selection. *Aust. Jnl. Of Bio. Sci.* 10:492.
48. Sastry, K., D. Goldberg, and G. Kendall. 2005. Genetic Algorithms. *In* Search Methodologies: Introductory Tutorials in Optimization and Decision Support Techniques. E. K. Burke and G. Kendall, eds Springer US, Boston, MA, pp. 97–125.
49. Wu, E. L., Y. Qi, …, W. Im. 2014. Preferred Orientations of Phosphoinositides in Bilayers and Their Implications in Protein Recognition Mechanisms. *J. Phys. Chem. B.* 118:4315–4325.

Please cite this article in press as: Huang and Chen, PIP2 regulation of TRPV4 channels: Binding sites and dynamic coupling, Biophysical Journal (2025), https://doi.org/10.1016/j.bpj.2025.08.006

50. Cover, T., and P. Hart. 1967. Nearest neighbor pattern classification. *IEEE Trans. Inf. Theor.* 13:21–27.
51. Hill, A. D., and P. J. Reilly. 2015. Scoring functions for AutoDock. *Methods Mol. Biol.* 1273:467–474.
52. Jo, S., T. Kim, and W. Im. 2007. Automated builder and database of protein/membrane complexes for molecular dynamics simulations. *PLoS One.* 2:e880.
53. Jo, S., J. B. Lim, …, W. Im. 2009. CHARMM-GUI Membrane Builder for mixed bilayers and its application to yeast membranes. *Biophys. J.* 97:50–58.
54. Klauda, J. B., R. M. Venable, …, R. W. Pastor. 2010. Update of the CHARMM all-atom additive force field for lipids: validation on six lipid types. *J. Phys. Chem. B.* 114:7830–7843.
55. Huang, J., S. Rauscher, …, A. D. MacKerell. 2017. CHARMM36m: an improved force field for folded and intrinsically disordered proteins. *Nat. Methods.* 14:71–73.
56. Abraham, M. J., T. Murtola, …, E. Lindahl. 2015. GROMACS: High performance molecular simulations through multi-level parallelism from laptops to supercomputers. *SoftwareX.* 1–2:19–25.
57. Hess, B., C. Kutzner, …, E. Lindahl. 2008. GROMACS 4: Algorithms for Highly Efficient, Load-Balanced, and Scalable Molecular Simulation. *J. Chem. Theor. Comput.* 4:435–447.
58. Darden, T., D. York, and L. Pedersen. 1993. Particle mesh Ewald: An N·log(N) method for Ewald sums in large systems. *J. Chem. Phys.* 98:10089–10092.
59. Ryckaert, J. P., G. Ciccotti, and H. J. C. Berendsen. 1977. Numerical integration of the cartesian equations of motion of a system with constraints: molecular dynamics of n-alkanes. *J. Comput. Phys.* 23: 327–341.
60. Berendsen, H. J. C., J. P. M. Postma, …, J. R. Haak. 1984. Molecular dynamics with coupling to an external bath. *J. Chem. Phys.* 81: 3684–3690.
61. Nosé, S. 1984. A unified formulation of the constant temperature molecular dynamics methods. *J. Chem. Phys.* 81:511–519.
62. Hoover, W. G. 1985. Canonical dynamics: Equilibrium phase-space distributions. *Phys. Rev. Appl.* 31:1695–1697.
63. Parrinello, M., and A. Rahman. 1981. Polymorphic transitions in single crystals: A new molecular dynamics method. *J. Appl. Phys.* 52: 7182–7190.
64. Torrie, G. M., and J. P. Valleau. 1977. Nonphysical sampling distributions in Monte Carlo free-energy estimation: Umbrella sampling. *J. Comput. Phys.* 23:187–199.
65. Kumar, S., J. M. Rosenberg, …, P. A. Kollman. 1992. The weighted histogram analysis method for free-energy calculations on biomolecules. I. The method. *J. Comput. Chem.* 13:1011–1021.
66. Michaud-Agrawal, N., E. J. Denning, …, O. Beckstein. 2011. MDAnalysis: A toolkit for the analysis of molecular dynamics simulations. *J. Comput. Chem.* 32:2319–2327.
67. Klesse, G., S. Rao, …, S. J. Tucker. 2019. CHAP: A Versatile Tool for the Structural and Functional Annotation of Ion Channel Pores. *J. Mol. Biol.* 431:3353–3365.
68. Humphrey, W., A. Dalke, and K. Schulten. 1996. VMD: visual molecular dynamics. *J. Mol. Graph.* 14:33-8–27-8.
69. Goretzki, B., C. Wiedemann, …, U. A. Hellmich. 2023. Crosstalk between regulatory elements in disordered TRPV4 N-terminus modulates lipid-dependent channel activity. *Nat. Commun.* 14:4165.
70. Goose, J. E., and M. S. P. Sansom. 2013. Reduced Lateral Mobility of Lipids and Proteins in Crowded Membranes. *PLoS Comput. Biol.* 9: e1003033.
71. Koldsø, H., and M. S. P. Sansom. 2012. Local Lipid Reorganization by a Transmembrane Protein Domain. *J. Phys. Chem. Lett.* 3:3498–3502.
72. Duneau, J.-P., J. Khao, and J. N. Sturgis. 2017. Lipid perturbation by membrane proteins and the lipophobic effect. *Biochim. Biophys. Acta Biomembr.* 1859:126–134.
73. Soom, M., R. Schönherr, …, S. H. Heinemann. 2001. Multiple PIP2 binding sites in Kir2.1 inwardly rectifying potassium channels. *FEBS Lett.* 490:49–53.
74. Driggers, C. M., Y.-Y. Kuo, …, S.-L. Shyng. 2024. Structure of an open KATP channel reveals tandem PIP2 binding sites mediating the Kir6.2 and SUR1 regulatory interface. *Nat. Commun.* 15:2502.
75. Pumroy, R. A., E. C. Fluck, …, V. Y. Moiseenkova-Bell. 2020. Structural insights into the gating mechanisms of TRPV channels. *Cell Calcium.* 87:102168.